℘

Stiff Response of Aluminum under Ultrafast Shockless Compression to 110 GPA

Raymond F. Smith,[1] Jon H. Eggert,[1] Alan Jankowski,[1] Peter M. Celliers,[1] M. John Edwards,[1] Yogendra M. Gupta,[2]
James R. Asay,[2] and Gilbert W. Collins[1]

[1]*Lawrence Livermore National Laboratory, P.O. Box 808, Livermore, California 94550, USA*
[2]*Washington State University, Pullman, Washington 99164, USA*

A laser-produced x-ray drive was used to shocklessly compress solid aluminum to a peak longitudinal stress of 110 GPa within 10 ns. Interface velocities versus time for multiple sample thicknesses were measured and converted to stress density ($P_x - \rho$) using an iterative Lagrangian analysis. These are the fastest shockless compression $P_x(\rho)$ results reported to date, and are stiffer than models that have been benchmarked against both static and shock-wave experiments. The present results suggest that at these short time scales there is a higher stress-dependent strength and a stiffer time-dependent inelastic response than had been expected.

Understanding the stress-strain ($\overleftrightarrow{\sigma} - \overleftrightarrow{\varepsilon}$) response of matter at extreme compressions is an important element of contemporary research in physics and materials science. Depending on the compression technique $\overleftrightarrow{\sigma} - \overleftrightarrow{\varepsilon}$ data can be obtained along very different and individually limited thermodynamic paths. Quasihydrostatic compression in diamond-anvil-cell (DAC) experiments typically provides isothermal data up to a pressure range of 200–300 GPa with experimental times ranging from seconds to days [1–3]. Shock-wave experiments, which uniaxially load material with a step function in time, can provide a single longitudinal stress-density ($P_x - \rho$) point along the shock adiabat to several TPa [4]. Here, $P_x = \sigma_{xx}$ and $\rho = \rho_o/(1 - \epsilon_{xx})$ due to inertial confinement. Shock compression produces a significant temperature increase so that at high stresses (>100 GPa) they sample very different regions of thermodynamic space than DAC experiments. Recently developed ramp-wave-loading experiments (commonly referred to as quasi-isentropic compression experiments, or ICE) permit the sampling of thermodynamic space not accessible by shock-wave or static pressure methods, ensure a solid state even at very high pressures, and provide data intermediate between shock-wave and static pressure results [5–12]. This Letter presents the first accurate $P_x - \rho$ data obtained on a laser-ICE platform. These are the fastest shockless compression $P_x(\rho)$ results reported to date, with compression times comparable to the intrinsic stress relaxation time.

Studies of time-dependent material response typically have used shock-wave experiments in which the compression consists of elastic and inelastic deformation and stress relaxation occurs on a time scale associated with lattice-dislocation mobility. At low stresses, an elastic wave, with a thickness-dependent amplitude, runs ahead of the plastic wave. At high stresses, a steady wave emerges with a rise time determined by a competition between the nonlinear stress-strain response and dissipative behavior [13]. What is the stress-strain response of a material shocklessly com-

pressed on a time scale comparable to the steady-shock rise time? The laser-driven ramp-compression experiments described uniaxially compress a material by applying a monotonically increasing stress over ∼10 ns, which is comparable to the low-stress steady-shock rise time for aluminum as reported by Swegle and Grady [13]. These new quasi-isentropic data reveal a stiffer response than expected from slower ramp-compression results and from models that have been benchmarked against both static and shock-wave experiments. Shockless compressions at these short time scales also produce precursor waves with amplitudes significantly higher than previously reported in shock and slower ramp-compression experiments. The ability to shocklessly compress materials to very high stresses on time scales comparable to dissipative relaxation times permits a new approach to explore the time-dependent deformation of materials at extreme conditions.

Shockless pressure loading techniques have been demonstrated using several drivers such as magnetic-pulse loading [5–7], graded-density-impactors on gas guns facilities [8], chemical energy of high explosives [9], and lasers [10–12]. The characteristic loading time for magnetic ramp loading is ∼100 ns, for graded-density-impactor loading is ∼1 μs, and for laser-ramp-loading is ∼10 ns. The capability of varying the ramp-compression time scales enables the study of time-dependent material behavior associated with structural changes and deformation in solids subjected to extreme compressions.

In previous laser-driven shockless compression experiments [10–12], the planarity of the pressure loading was limited by laser focal-spot smoothing techniques, which precluded their use for equation-of-state (EOS) measurements. Here, we have developed a laser-produced x-ray drive technique to generate ramp-wave loading that was spatially uniform to <1% over 500 μm. This uniform loading ensured that different thicknesses of multistep targets had the same loading history. A target layout is shown in Fig. 1(a). Fifteen beams from the Omega laser, with a combined energy of up to 5.9 kJ in a 2 ns temporally
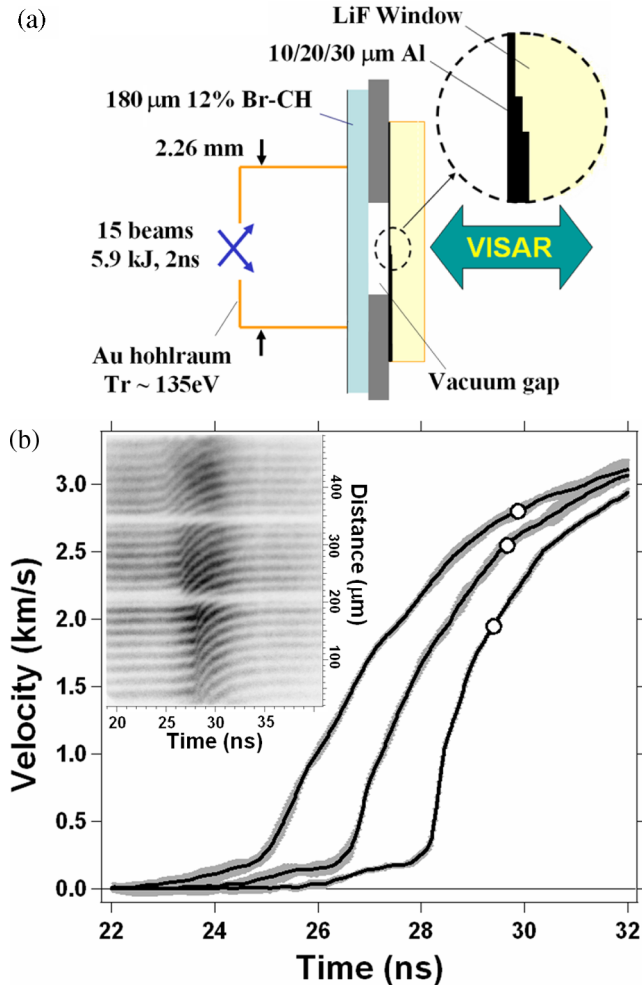
(a)

(b)

FIG. 1 (color online). (a) X-ray-driven laser-ICE-EOS target sketch. (b) Interface-velocity history for each step of the Al/LiF example. The width of the curves shows the random uncertainty of the measurement. The black line shows the forward propagated velocity determined from the load pressure history and the measured $C_L(u)$.

flat pulse, were focused onto the inner walls of an Au hohlraum. This generated a uniform distribution of thermal x rays with a peak radiation temperature, Tr = 135 eV as measured with a calibrated array of filtered diodes. An ablatively driven shock runs through a 180 μm-thick, 12% Br-doped polystyrene foil [$C_8H_6Br_2$]. After shock breakout from the rear surface, the CH-Br unloading plasma crosses a ~400 μm vacuum gap and piles up against the multistep Al sample launching a ramped stress wave. The vacuum gap, Tr, and Al thicknesses were tuned to optimize the pressure and accuracy. The Bromine dopant absorbs high energy Au M-band x rays generated within the hohlraum which otherwise could preheat the Al step sample. The level of x-ray preheat was determined to be negligible by measuring the thermal expansion velocity of a thin Al foil under the target and irradiation conditions described here [14].

Al samples were either a 10, 20, and 30 μm thick stepped foil attached to a LiF window or a 40, 60, and 80 μm freestanding stepped foil. For Al/LiF samples, Al was coated directly onto stepped LiF windows with electron-beam deposition at a growth temperature of 425 K. For freestanding samples, Al was deposited onto a salt mandrel in a similar way and then the mandrel was removed. Optical imaging of the samples showed a tightly packed ~5 μm long tapered-crystallite structure in the stress-loading direction with an average in-plane grain size of ~1.5 ± 0.3 μm. Bragg diffraction showed a preferential [111] fcc structure in the growth direction. Samples were measured to be fully dense (2.7 g/cc) to within an accuracy of −0.6%. The source Al was 99.999% pure [15]. After deposition, the Al surface away from the mandrel was diamond turned to achieve planarity. Through each stage of the process, white-light interferometry was used to ensure a surface roughness <0.1 μm, overall thickness gradients <1%, and step heights <1%. The high purity LiF was orientated with the [100] axis along the pressure loading direction.

As the particle-velocity wave reaches the back surface of the Al, it begins to accelerate into the LiF window or into free space. The interface-velocity history $u_{Al/LiF}$ or u_{fs}, is recorded with a line-imaging velocity interferometer (VISAR) with two channels set at different sensitivities [16]. The inset of Fig. 1(b) shows a typical streak camera output of the VISAR for an Al/LiF target. The spatial resolution is ~5 μm over ~500 μm at the target plane. The temporal resolution is 50 ps over a 30 ns time window. The minimum velocity per fringe was 0.645 km s^{-1} and we detect fringe position to 5% of a fringe. Figure 1(b) shows representative interface-velocity histories for each of the 10, 20, and 30 μm thick steps. For all Al/LiF samples, we observed a low amplitude precursor similar to the elastic precursor in shock experiments [17]. This velocity plateau corresponds to P_x ~ 2.7 GPa, which is significantly higher than the reported Hugoniot elastic limit for pure Al (~0.15 GPa) on millimeter-scale thick targets [17] and 17 times higher than quasistatic tensile measurements on the same material used here.

An iterative characteristic method outlined by Maw and Rothman [18] is used to convert interface-velocity histories to particle velocity, u. One central assumption for all current ramp-wave-analysis techniques is that the ramp wave is a simple wave. This implies [19] that the stress and particle-velocity propagation speeds are identical and equal to $C_L(u)$. For Al/LiF targets, the measured interface velocity is very close to the *in situ* particle velocity due to the comparable mechanical impedance of LiF and Al. Furthermore, the refractive index of LiF depends linearly on density in this regime, so the index correction for the velocity calibration is trivial [20]. However, late in time a shock forms in the LiF producing a release fan, which propagates back to and accelerates the Al/LiF interface. At this point the analysis becomes more difficult and so

was terminated for these experiments. The open circles Fig. 1(b) show where the release from shock formation in the LiF reaches the Al/LiF interface, as determined from the characteristic analysis. For Al/vacuum targets, release waves from the Al/vacuum interface significantly perturb the incoming ramp wave. Extensive tests using simulated data confirm that the iterative Lagrangian analysis accurately corrects for these wave interactions. When the release wave reflects from the drive surface and reaches the Al/vacuum interface again, the analysis is stopped due to an increase in velocity that is not accounted for with present analysis techniques.

The iterative Lagrangian analysis gives a time for a given particle velocity, u, to reach each step. The Lagrangian sound speed, $C_L(u)$, and its uncertainty, $\sigma_{C_L}(u)$, are obtained from this position-time data by linear regression using errors determined by measurements accuracies: u (~0.1 km/s), time (~50 ps), step height (~1%). $C_L(u)$ for each of the 7 independent experiments (5 with LiF windows and 2 free surfaces) taken over three different shot days are shown in the inset of Fig. 2. To our knowledge, the present work represents the first comparison of different ramp-loading experiments to evaluate systematics. That the Al/vacuum and Al/LiF targets yield the same value for $C_L(u)$ demonstrates that the methodology for correcting for the strong release effects is indeed consistent. By inspection we find that the experimental uncertainty in the analysis of each shot is very consistent with the shot-to-shot scatter. Thus, we have calculated the

weighted mean,

$$\langle C_L \rangle = \sum_j \frac{C_{L,j}}{\sigma_{C_L,j}^2} \bigg/ \sum_j \frac{1}{\sigma_{C_L,j}^2},$$

and uncertainty in the mean,

$$\sigma_{\langle C_L \rangle} = \left(1 \bigg/ \sum_j \frac{1}{\sigma_{C_L,j}^2} \right)^{1/2},$$

as shown in Fig. 2. For $u > 0.5$ km/s the weighted mean can be linearly extrapolated to a value close to the bulk sound speed (open circle) [3]. For values of $u < 0.5$ the weighted mean extrapolates closer to the longitudinal sound speed (green circle) [21]. For particle speeds <0.2 km/s, C_L is dominated by elastic deformation.

$\langle C_L \rangle$ and $\sigma_{\langle C_L \rangle}$ are integrated [18,19] to obtain $P_x = \rho_0 \int_0^u \langle C_L \rangle du$, $\rho = (\frac{1}{\rho_0} - \frac{1}{\rho_0} \int_0^u \frac{du}{\langle C_L \rangle})^{-1}$, and their uncertainties, $\sigma_{P_x} = \rho_0 \int_0^u \sigma_{\langle C_L \rangle} du$, $\sigma_\rho = \frac{\rho^2}{\rho_0} \int_0^u \frac{\sigma_{\langle C_L \rangle} du}{\langle C_L \rangle^2}$. Uncertainties are propagated through the integrals linearly, rather than in quadrature, because $\sigma_{\langle C_L \rangle}$ appears to be correlated rather than random over the ramp wave. This method of uncertainty propagation allows the direct propagation of experimental uncertainties to the $P_x - \rho$ density relation.

The resultant P_x versus ρ are shown in Fig. 2. Stress-density results reported here are stiffer than results recently published from pulsed power experiments by Davis [5]. One possible reason for this difference is that our ramp times (~10 ns) and thicknesses (tens of microns) are 10 to 100 times less than previous ramp-wave compression experiments and our compression times are similar to the
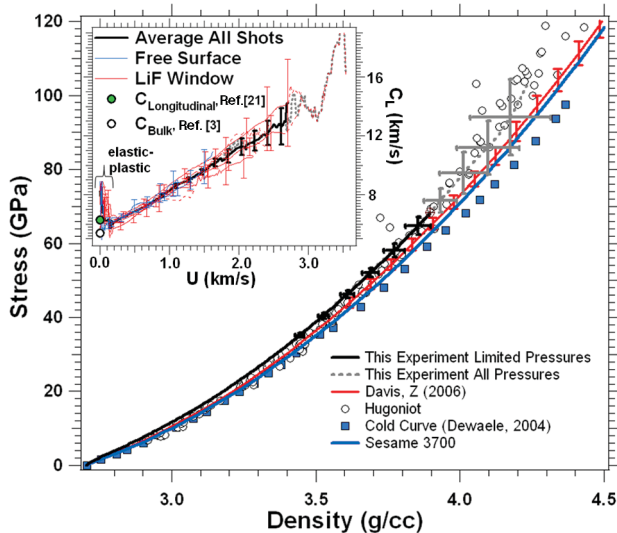

FIG. 2 (color). Quasi-isentropic stress versus density data presented here together with previous data from Davis [5]. Also shown are Hugoniot [4] and cold curve data [2], and a calculated isentrope from the 3700 EOS model from the Sesame database [22]. The inset shows $C_L(u)$ for all seven shots. The black line represents the weighted mean $\langle C_L \rangle$ for all shots with the analysis limited to times preceding the influence of the LiF shock or reverberations in the case of Al/vacuum targets. The gray dashed line represents the weighted mean over the entire profile.
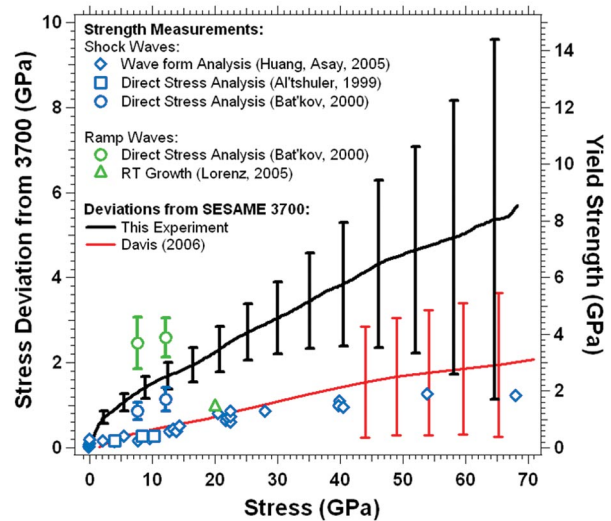

FIG. 3 (color). Extra stress versus nominal stress determined by subtracting our measured quasi-isentrope from the isentrope calculated from the table 3700 from the Sesame library [22]. The right-hand axis is the same but magnified by 3/2 to enable comparison with previous yield strength results. Also shown are the strength measurements from shock waves of Huang [17], Al'tshular [26], and Bat'kov [27], and ramp-load data from Lorenz [11] and Bat'kov [27]. The black line corresponds to the analysis region described for $C_L(u)$ inset plot in Fig. 2.

PHYSICAL REVIEW LETTERS

steady wave rise times under shock loading. Unlike the analysis described here the Lagrangian analysis by Davis [5] did not include the low velocity precursor observed in the experiments. Also shown for comparison are Hugoniot results from several authors [4], the cold curve from Dewaele *et al.* [2], and the isentrope calculated from the EOS model 3700 from the Sesame database [22]. Sesame 3700 has previously been shown to give good agreement with Hugoniot data up to several hundred GPa [4,23].

Figure 3 accentuates the differences shown in Fig. 2, by plotting the stress deviation between the P_x values and the isentrope calculated from the Sesame 3700 EOS table. In the analysis of Fowles [24] using the Lévy–von Mises yield criterion [25] this stress deviation corresponds to two-thirds the yield strength. Using this relationship, assuming that the isentrope calculated using Sesame 3700 is correct, and assuming the additional longitudinal stress is dominated by strength effects, the maximum value for the yield strength can be obtained in Fig. 3 by reading off the right-hand axis. While the stress deviation is not an absolute measurement of strength, it is instructive to present the data in this way to compare against previous work. The stiffer than expected response at high stress is analogous to the much higher precursor observed in these rapidly ramp loaded data as compared to previous measurements. Also plotted in Fig. 3 are yield strength data from several authors. The stress difference observed in the present experiments is higher than expected from shock-wave strength determinations by Huang and Asay [17], Al'tshuler [26], and ramp-load results of Lorenz *et al.* [11] but lower than expected from results of Bat'kov [27]. While the Bat'kov results are systematically high compared to other results, the difference between their ramp and shock results are comparable to the difference between our ramp-load results and the shock results in Refs. [17,26].

In summary, results presented here represent a systematic study of the quasi-isentropic behavior of Al at strain rates approaching $10^8/s$ [28] and provide $P_x - \rho$ results to 110 GPa. In the predominately plastic regime, P_x is larger than expected by ~5–6 GPa at ~70 GPa, suggesting a higher stress-dependent strength and a larger than expected time-dependent deformation response at these short time scales. In addition, the elastic precursor stress for Al/LiF samples is nearly 7 times higher than previously reported in ramp- and shock-wave experiments [29]. Further experimental, analytical, and theoretical work is needed to understand the results presented here. However, it is clear that ramp-wave experiments, with rise times comparable to material dissipation times, have the potential to provide new insights into the dynamic response of materials at extreme conditions.

[1] L. S. Dubrovinsky *et al.*, Phys. Rev. Lett. **84**, 1720 (2000).
[2] A. Dewaele *et al.*, Phys. Rev. B **70**, 094112 (2004).
[3] A. D. Chijioke *et al.*, J. Appl. Phys. **98**, 073526 (2005).
[4] See P. M. Celliers *et al.*, J. Appl. Phys. **98**, 113529 (2005), and references within.
[5] J.-P. Davis, J. Appl. Phys. **99**, 103512 (2006).
[6] D. B. Hayes *et al.*, J. Appl. Phys. **96**, 5520 (2004).
[7] (a) R. S. Hawke *et al.*, J. Appl. Phys. **43**, 2734 (1972); (b) J. R. Asay, in *Shock Compression of Condensed Matter—1999*, edited by M. D. Furnish *et al.*, AIP Conf. Proc. No. 505 (AIP, New York, 2000), p. 261.
[8] L. C. Chhabildas and L. M. Barker, Sandia Report No. SAND86-1888, 1986; J. R. Asay, Int. J. Impact Eng. **20**, 27 (1997).
[9] J. F. Barnes *et al.*, J. Appl. Phys. **45**, 727 (1974).
[10] M. J. Edwards *et al.*, Phys. Rev. Lett. **92**, 075002 (2004).
[11] K. T. Lorenz *et al.*, Phys. Plasmas **12**, 056309 (2005).
[12] D. C. Swift and R. P. Johnson, Phys. Rev. E **71**, 066401 (2005).
[13] J. W. Swegle and D. E. Grady, J. Appl. Phys. **58**, 692 (1985).
[14] R. F. Smith *et al.*, Phys. Plasmas (to be published).
[15] The source aluminum was supplied by Williams Advanced Materials, Inc., Santa Clara, CA 95054, USA.
[16] P. M. Celliers *et al.*, Rev. Sci. Instrum. **75**, 4916 (2004).
[17] H. Huang and J. R. Asay, J. Appl. Phys. **98**, 033524 (2005).
[18] J. R. Maw, in *Shock Compression of Condensed Matter—2003*, edited by M. D. Furnish *et al.*, AIP Conf. Proc. No. 706 (AIP, New York, 2004), p. 1217; S. D. Rothman *et al.*, J. Phys. D **38**, 733 (2005).
[19] J. B. Aidun and Y. M. Gupta, J. Appl. Phys. **69**, 6998 (1991); R. Fowles and R. F. Williams, J. Appl. Phys. **41**, 360 (1970); M. Cowperthwait and R. F. Williams, J. Appl. Phys. **42**, 456 (1971).
[20] D. B. Hayes, J. Appl. Phys. **89**, 6484 (2001).
[21] S. Marsh, *LASL Shock Hugoniot Data* (University of California Press, Berkeley, 1980).
[22] G. I. Kerley, Int. J. Impact Eng. **5**, 441 (1987); S. P. Lyon and J. D. Johnson, Los Alamos Report No. LA-CP-98-100, 1998. The Al EOS developed by Kerley is used at the Sandia National Laboratories and commonly referred to as the 3700 table.
[23] M. D. Knudson *et al.*, J. Appl. Phys. **97**, 073514 (2005).
[24] G. R. Fowles, J. Appl. Phys. **32**, 1475 (1961).
[25] R. Hill, *The Mathematical Theory of Plasticity* (Oxford University Press, New York, 1950).
[26] L. V. Al'tshuler, Combust. Explos. Shock Waves **35**, 92 (1999).
[27] Y. V. Bat'kov *et al.*, in *Shock Compression of Condensed Matter—1999* (Ref. [7(b)]), p. 501.
[28] The strain rate $d\eta/dt \equiv [du/dt]/[C_L(u)]$, where the strain η is positive under compression and u is the particle velocity. We find $d\eta/dt$ increases from $10^6/s$ at a few GPa to $10^8/s$ at ~5 GPa, and then drops slowly above 5 GPa.
[29] The previous experiments used Al 6061 with a grain size of a few hundred μm in contrast to the pure Al with ~5 μm columnar crystals used in this study.